applied sciences

MDPI

Article

Water-Weakening Effects on the Mechanical Behavior of Different Rock Types: Phenomena and Mechanisms

Xin Cai [1], Zilong Zhou [1,2,*], Kewei Liu [1,*], Xueming Du [1,3,*] and Haizhi Zang [4]

1 School of Resources and Safety Engineering, Central South University, Changsha 410010, China; xincai@csu.edu.cn
2 College of Civil Engineering and Architecture, Hainan University, Haikou 570000, China
3 College of Water Conservancy and Environmental Engineering, Zhengzhou University, Zhengzhou 450001, China
4 ARC Centre of Excellence for Geotechnical Science and Engineering, Faculty of Engineering and Built Environment, The University of Newcastle, Callaghan 2308, Australia; zang8111616@163.com
* Correspondence: zlzhou@csu.edu.cn (Z.Z.); kewei_liu@csu.edu.cn (K.L.); 2007-dxm@163.com (X.D.)

Received: 29 August 2019; Accepted: 16 October 2019; Published: 20 October 2019

check for updates

Abstract: The presence of water strongly affects rock properties and would be related to a series of geological disasters. To understand water saturation effects on the mechanical behavior of different rock types and interpret the underlying mechanisms of differences in water sensitivity, three kinds of rocks, namely sandstone, granite and marble, were selected for tests. Uniaxial compression experiments were conducted on specimens under oven-dried and water-saturated conditions. Acoustic emission (AE) techniques were also applied to monitor and record AE signals during tests. Experimental results reveal that water weakens the mechanical parameters of the three tested rocks, such as uniaxial compressive strength (UCS), elastic modulus and critical strain. The sandstone undergoes the greatest weakening with the addition of pore water, the mechanical properties of the granite exhibit relatively minor reductions, while the marble is the least affected by water saturation. The water-weakening degree of rock properties depends on the porosity as well as the mineralogy, especially the proportion of quartz and swelling clays. Moreover, after water saturation, the failure pattern of the sandstone and the granite tends to transform into the shear-dominant mode from the tensile one in dry state, probably due to frictional reduction. However, the water presence does not change the failure mode of the marble.

Keywords: water weakening; failure type; mineral composition; quartz hydrolysis; pore pressure; frictional reduction

1. Introduction

The presence of water can markedly alter the mechanical behavior of rock materials [1–7], which are responsible for a variety of geological disasters such as landslides [8], goaf collapse [9,10] and fault activation [11–13]. In many engineering applications such as tunnels, mines, basements and radioactive waste storage, rocks are commonly subjected to water erosion resulting from construction beneath the groundwater table. The properties of constructional materials under such conditions are expected to be significantly different from those in a dry state. Therefore, it is crucial to investigate the water saturation effects on the mechanical behavior of rocks for the design and construction of underground rock engineering.

Massive efforts have been made to explore the water-induced changes in rock properties [1–6,14–28]. Among them, the effects of water on the uniaxial compressive behavior, such as the uniaxial compressive strength (UCS) and elastic modulus, are more commonly studied than other mechanical parameters due to their most direct, practical relevance to rock engineering applications [7]. Over several decades, uniaxial compression tests have been conducted on a large variety of rock types under different moisture conditions, involving igneous rocks [25,26], sedimentary rocks [1,3,4,14–16,27,28] and metamorphic rocks [2,29,30]. For instance, Dyke and Dobereiner [15] in 1991 reported that an increase in water content tends to reduce rock strength. They suggested that the interaction between water and silicate minerals converts strong silicon–oxygen bonds to weaker hydrogen bonds, decreasing the strength of quartz-rich sandstones. Similarly, Hadizadeh and Law [27] investigated the water-weakening effects on the UCS and stiffness of the Pennant sandstone and the Oughtibridge ganister. They speculated that the intrinsic microfabric of rock (e.g., porosity, geometry of grain boundary and grain–matrix relationships) significantly affects the water sensitivity of rock strength. Hawkins and McConnell [1] further investigated the sensitivity of strength and deformability of 35 British sandstone types to variable water content. They observed that the UCS of sandstones follows a negative exponential relationship with water content. They also found that the degree of sensitivity to water content is primarily controlled by the mineral composition, particularly the abundance of quartz and clay minerals, and to a lesser extent by the rock fabric. Erguler and Ulusay [2] showed that the UCS and elastic modulus of clay-bearing rocks can decrease up to 90% and 93%, respectively, with the increasing water content. They also established empirical models to estimate the water sensitivity of clay-bearing rocks using coefficients relevant to physical properties of the rocks such as porosity, dry unit weight and water absorption. Jiang et al. [16] discovered that the UCS of mudstone decreases to only 5 MPa after immersed in water for one month, from 45 MPa under a dry condition. Additionally, they employed X-ray diffraction and scanning electron microscopy to examine the real-time mudstone–water interaction. They concluded that water-induced deterioration processes for mudstone can be divided into three stages: water firstly invades into the rock specimen from initial defects; then water gives rise to the dissolution of carbonate cement and the volumetric swelling of clay minerals by physical and chemical reactions; finally, these effects facilitate the propagation and interconnection of microcracks within rocks.

It is universally acknowledged that the presence of water weakens the strength and stiffness of rock materials under quasi-static compression. To further reveal the loss degree of UCS induced by water saturation, the test data on the UCS of rocks in dry and saturated states were compiled and analyzed from hundreds of studies according to the calculating method proposed by Wong et al. [7]. The percentage distribution of UCS reduction for different rock types is shown in Figure 1. Evidently, the water-weakening extent on rock strength is highly dependent on the rock type, and likely reflects the great differences in lithology and texture. The UCS losses in the vast majority of rocks fall in the range from 0% to 60%. Compared to metamorphic and igneous rocks, sedimentary rocks generally suffer greater reductions in UCS. However, rock strength is susceptible to the test conditions [7,24,31,32] such as strain rate, loading apparatus and ambient temperature. Test conditions are usually different between experiments. This results in the low degree of comparability of tested data. Hence, there is a need to research the UCS sensitivities to water of varied rock types under the same test conditions.

To date, many mechanisms have been proposed to explain the water-induced strength reduction, such as fracture energy reduction [6,33,34], chemical and physical deterioration [35–38], pore pressure increase [39,40], capillary tension decrease [41] and frictional reduction [42–46]. Several mechanisms may act concurrently to control the deformation of wet rocks. However, none of these mechanisms can be uniquely determined for the great variety of rock types, but one or some are likely more significant than others for certain rock types and test conditions [7,42,47].

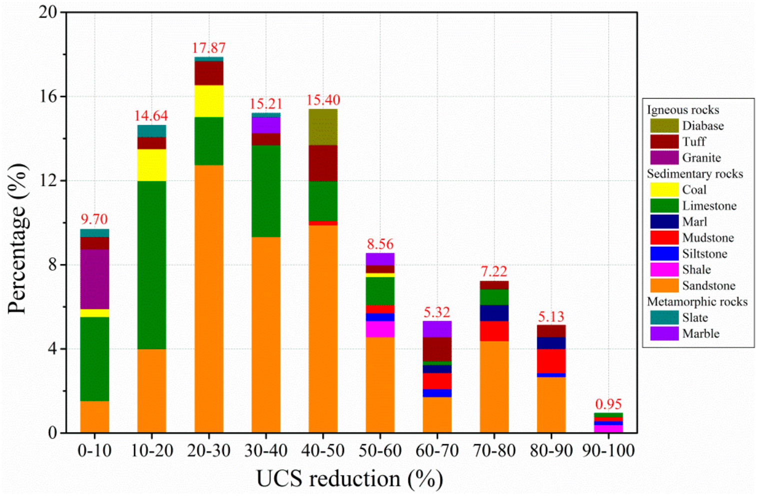

Figure 1. Percentage distribution of uniaxial compressive strength (UCS) reduction induced by water saturation for different rock types (red numbers denote the total percentage falling under a specific range of UCS reduction for various rock types).

In this paper, to explore the water effects on the mechanical behavior of various rocks, three types of rock, namely sandstone, granite and marble, were selected as test materials. Uniaxial compression tests were performed on three rock types under dry and saturated conditions. Mechanical parameters such as UCS, elastic modulus and critical strain were obtained and then compared. The damage evolution within rocks during deformation was monitored by the acoustic emission (AE) technique. The different UCS sensitivities to water of different rock types were explained in terms of the differences in the minerology and texture.

2. Test Material and Method

2.1. Material Characterization

Three rock types commonly encountered in rock engineering applications were chosen for experiments, i.e., one igneous rock (granite), one sedimentary rock (sandstone) and one metamorphic rock (marble). The sampling locations for the three rocks are shown in Figure 2. We conducted X-ray diffraction (XRD) and thin section analysis to obtain the accurate petrologic compositions of the tested materials. Table 1 shows the constituent mineralogical components and their proportions.

The sandstone was collected from Chuxiong, Yunnan province, China. It consisted of 57.20% quartz, 13.48% feldspar, 5.26% calcite, 3.84% mica and 13.77% clay minerals (9.72% of the sample being smectite and 4.05% being chlorite). The main cement was calcite. The granite was collected from Yueyang, Hunan province, China. It comprises 38.77% feldspar, 32.82% quartz, 22.85% muscovite and 5.56% chlorite. The marble was collected from Hengyang, Hunan province, China. Within the marble, dolomite (96.98%) grains are dominant, in which a little calcite (3.02%) is dispersedly embedded.

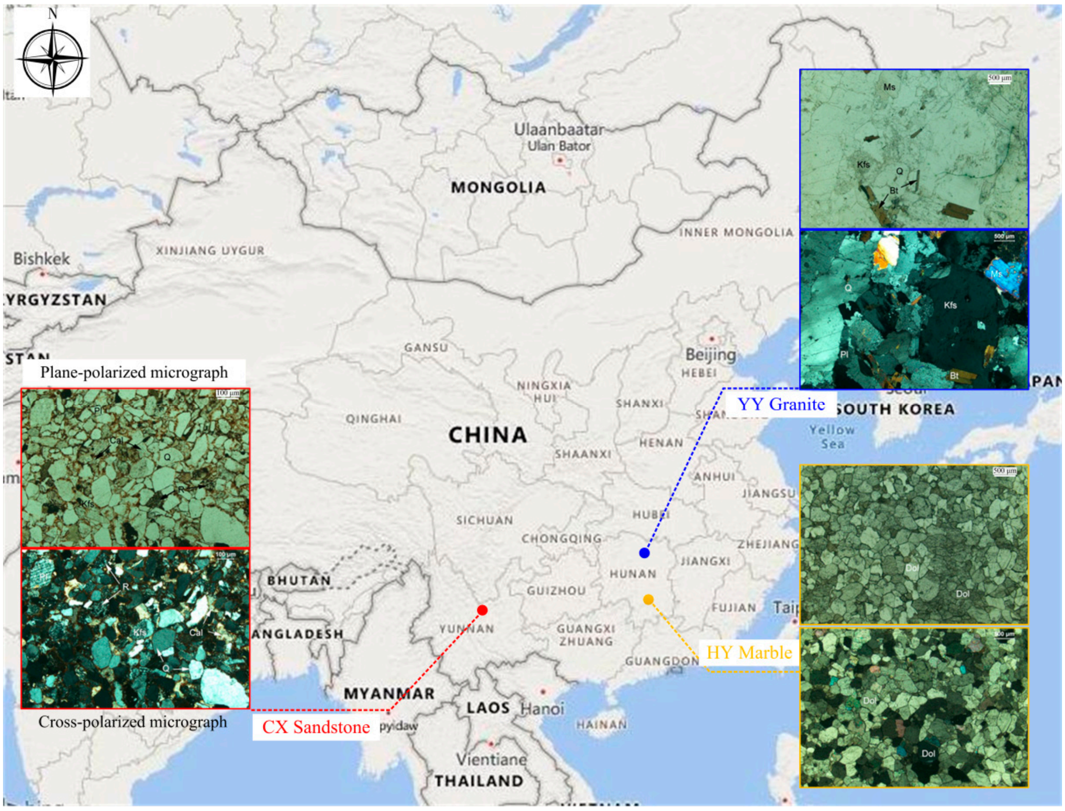

Figure 2. Sampling locations of the tested rocks and optical polarized micrographs for each rock.

Table 1. Percentage and grain size of mineralogical compositions for three rock types.

Rock Type	Mineral Composition	Percentage [a]/%	Grain Size [b]/mm	Average Grain Size/mm
Sandstone	Quartz	57.20	0.02–0.25	0.055
	Feldspar	13.48	0.05–0.24	
	Calcite	5.26	0.01–0.15	
	Mica	3.84	0.04–0.14	
	Smectite	9.72	0.01–0.03	
	Chlorite	4.05	0.01–0.05	
Granite	Feldspar	38.77	0.1–2.5	1.970
	Quartz	32.82	0.2–2.2	
	Muscovite	22.85	0.05–2.2	
	Chlorite	5.56	0.01–0.2	
Marble	Dolomite	96.98	0.1–0.6	0.083
	Calcite	3.02	0.1–0.4	

[a] The percentage of mineral compositions was determined by X-ray diffraction technique. [b] The grain size was measured by optical micrographs.

Mean grain sizes were measured using optical polarized micrographs of thin sections. The test results exhibit mean grain sizes of 0.055, 1.970 and 0.083 mm for the sandstone, the granite and the marble, respectively. Nuclear magnetic resonance (NMR) tests were also carried out to determine rock porosities. The porosities of the sandstone, the granite and the marble were 8.50%, 1.07% and 0.63%, respectively. More essential physical parameters are listed in Table 2.

Table 2. Some essential physical and mechanical parameters of tested rocks.

Rock Type	State	ϕ /%	ρ /kg·m^{-3}	A_w /%	t_s [a] /h	C_p /m·s^{-1}	κ /nm^2	K /GPa
Sandstone	Dry Sat.	8.50	2368.5 2453.5	0.00 2.29	48	3094.0 3614.5	3.76×10^2	4.70 N.A.
Granite	Dry Sat.	1.07	2620.3 2625.8	0.00 0.52	168	4333.4 5105.6	0.23	12.24 N.A.
Marble	Dry Sat.	0.63	2821.2 2824.6	0.00 0.13	168	5241.5 6498.9	1.72×10^{-2}	14.91 N.A.

Note: ρ, density; ϕ, porosity; A_w, water absorption; t_s, time required for saturation via water immersion; C_p, primary wave velocity; κ, permeability; K, bulk modulus; N.A., not available. [a] The time for water saturation was determined by monitoring the weight variation of the rock [4,48]. The specimen was considered to reach a fully saturated state once its weight did not increase with time.

2.2. Specimen Preparation

Specimens were obtained from small-scale slabs of each rock type without visible geological weakness (e.g., fractures and lamination) [49]. Rectangular prisms with the dimensions of $50 \times 50 \times 100$ mm^3 were first sliced. The end surfaces of each specimen were then polished perpendicular to the long axis. To minimize the variation of physical properties across the specimen set, P-wave measurements were conducted after specimen preparation. Specimens with similar wave velocities were chosen for further analysis.

For each rock type, a total of ten specimens were selected for tests. Half of them were designed to be tested under dry conditions and the remaining specimens were tested under water-saturated conditions. Firstly, all specimens were stored in an oven at the constant temperature of 105 °C more than 48 h to assure complete dryness. Afterwards, half of them were submerged in water for at least the time required for full saturation as shown in Table 2. To avoid the moisture exchange between rock specimen and environment, the dry specimens were wrapped by plastic film and the saturated specimens were placed in a water tank before experiments.

2.3. Experimental Techniques and Test Condition

Uniaxial compression tests were conducted on an electric servo-hydraulic material testing machine (INSTRON 1346) installed at the Advanced Research Center in Central South University. A load cell and a linear variable differential transformer were applied to monitor and record the axial force and displacement, respectively, on the specimen at 100 Hz logging frequency. Silicon grease lubricant was elaborately smeared on the platens and the top and bottom surfaces of specimens to reduce the end friction on the specimen–platen interfaces.

An acoustic emission (AE) system manufactured by Physical Acoustic Corporation was used for the acquisition and analysis of the microcrack evolution within the specimen during the loading process. A pair of AE sensors (Nano 30) mounted on the specimen surfaces and pre-amplifiers were adopted to monitor the AE events from the specimens. The threshold value of 45 dB was set to avoid the disturbance of outside noises, i.e., a signal is identified as an AE event and acquired only when its amplitude exceeds 45 dB. Otherwise, it will be eliminated. In each test, the INSTRON and the AE system were manually triggered synchronously.

To minimize the data discreteness, all specimens were tested under the same conditions. The constant strain rate of 4×10^{-5} s^{-1} was designed for testing all specimens. The axial displacement rate was thus controlled at 0.24 mm·min^{-1} until specimen failure. Moreover, by means of the air conditioner, the temperature in the laboratory was kept at 25 °C and the humidity was maintained at 60%.

3. Test Results

This section presents the analysis of the test results of different rock types in oven-dried and water-saturated states under two sub-sections: (1) mechanical behavior and (2) AE characteristics.

3.1. Effect of Water on Mechanical Behavior

3.1.1. Stress–Strain Response of Dry and Saturated Rocks

Figure 3 depicts typical stress–strain curves for different rock types tested under dry and saturated conditions. The peak stresses of the sandstone and granite significantly decreased after water saturation. However, the water-weakening effect on the peak stress of the marble was not obvious. After peak stress, all specimens exhibited catastrophic stress drop. Obviously, the declining slopes of dry specimens are greater than that of saturated ones, indicating that water made the rocks more ductile.

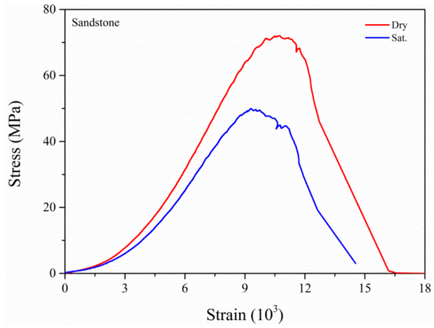

(**a**)

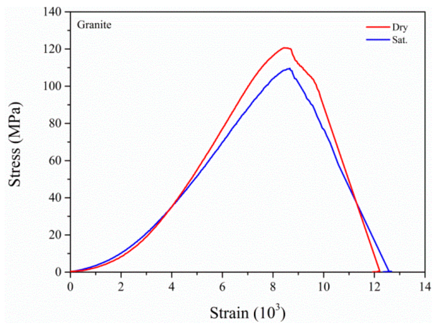

(**b**)

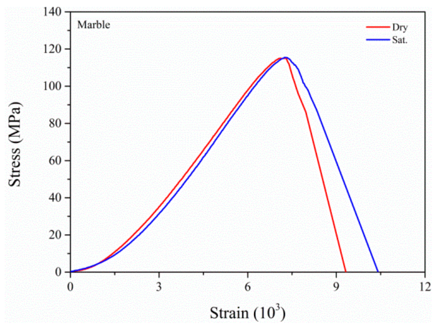

(**c**)

Figure 3. Stress–strain curves of (**a**) sandstone; (**b**) granite; and (**c**) marble under dry and water-saturated conditions.

3.1.2. Water-Weakening Effect on Mechanical Behavior

Table 3 lists the average value of the mechanical properties (i.e., UCS, elastic modulus and critical strain) obtained from the stress–strain relationships. The UCS is the maximum stress exerted on specimens, the elastic modulus is the slope of linear portion in the curves, and the critical strain is the strain of specimen at the peak stress. It can be clearly seen that the mechanical parameters of the three rock types decreased under water saturation conditions.

Table 3. Average values of tested data.

Rock Type	State	t_f /s	σ_c /MPa	E /GPa	ε_c /‰	N_c /10^3
Sandstone	Dry	253.0	71.91	7.05	10.21	18.0
	Sat.	225.9	50.48	5.52	9.16	3.7
Granite	Dry	216.6	123.82	15.18	8.46	985.7
	Sat.	204.8	119.39	14.34	8.32	184.5
Marble	Dry	174.0	119.48	16.82	7.12	8.1
	Sat.	176.5	118.77	16.78	7.08	5.9

t_f, time-to-failure; σ_c, uniaxial compressive strength; E, elastic modulus; ε_c, critical strain; N_c, cumulative ring counts.

Figure 4a illustrates that the uniaxial compressive strengths (UCSs) of all three types of rocks were reduced by water. Among the three tested rock types, the sandstone specimen underwent the largest drop in UCS due to water saturation. The average UCS of the dry sandstone specimen was 71.91 MPa. After soaking, the average UCS of the sandstone specimen was reduced to 50.48 MPa. For the granite, the average UCS of the saturated specimen decreased to 119.39 MPa from 123.82 MPa in the dry state. There was a negligible UCS reduction for the marble, indicating that the strength of the marble was not apparently affected by water. Apart from the reduction in the average UCS, the standard deviation of the average UCS also decreased after water saturation. The average UCSs of dry sandstone, granite and marble specimens possessed standard deviations of 0.27, 6.34 and 1.26 MPa, respectively. The UCS standard deviations of saturated sandstone, granite and marble specimens were 0.16, 5.70 and 0.49 MPa, respectively. The tested UCS values were less scattered for saturated rocks compared to dry ones.

Figure 4b displays the elastic modulus of dry and saturated rocks. The elastic modulus followed a similar weakening trend as UCS. The elastic modulus of all three rock types also decreased after water saturation. The reduction in the elastic modulus of the sandstone was considerable, and that of the granite was relatively minor, while that of the marble was not apparent.

Figure 4c exhibits the water-induced variation of critical strain. Under saturated condition, the loss in the critical strain was noteworthy for the sandstone compared to the relatively small reductions for the granite and the marble.

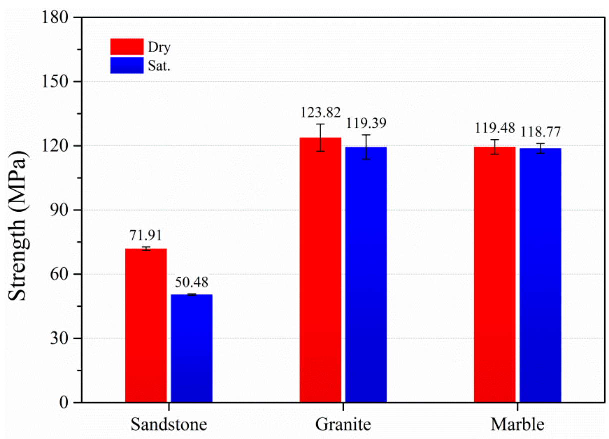

(**a**)

Figure 4. *Cont.*

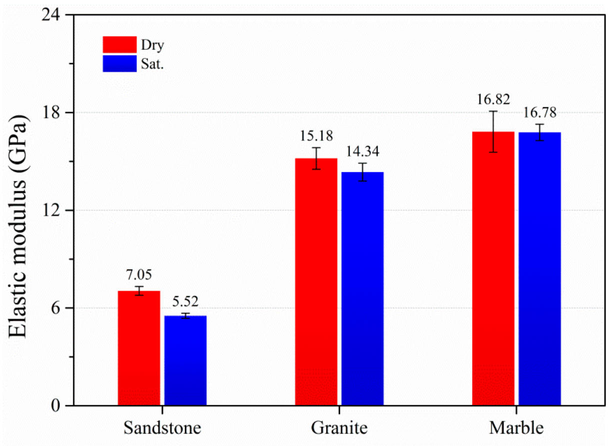

(**b**)

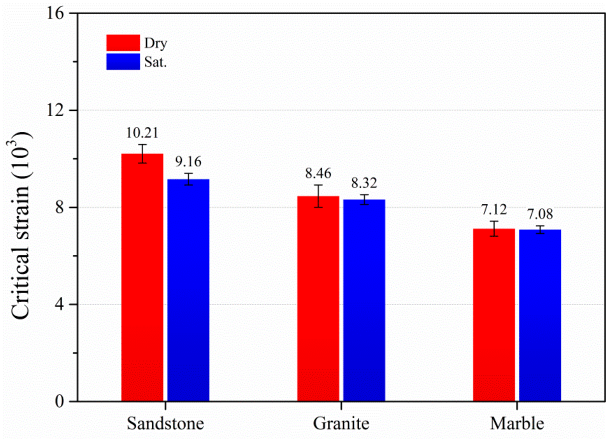

(**c**)

Figure 4. Water-induced changes in mechanical properties of three rock types: (**a**) uniaxial compressive strength; (**b**) elastic modulus; and (**c**) critical strain.

3.2. Effect of Water on AE Characteristics

3.2.1. Cumulative and Evolution of Ring Counts

Ring counts and their cumulative value are the main indexes to characterize the damage evolution within rock materials [50]. Figure 5 demonstrates the variations of axial stress, ring counts and cumulative ring counts versus time. Obviously, the history of ring counts for all specimens showed similar trends regardless of rock type and moisture condition. According to the occurrence of ring counts and the slope of stress history, we can divide the loading process into four stages:

(1) Crack closure stage (stage I), where initial defects are closed, and the stress increases slowly. In theory, very few or even no ring counts occur because of little energy release during this stage [23,48,51].
(2) Elastic deformation stage (stage II), where the rock specimen deforms elastically. The stress increases linearly accompanied by the slow and stable accumulation of ring counts. This implies that microcracks initiate steadily.
(3) Unstable crack propagation stage (stage III), where ring counts exponentially burst with the increasing stress due to the energy storage enough to trigger the eruption of microcracks.
(4) Post-peak stage (stage IV), where the stress drops suddenly with the majority of ring counts occurrence.

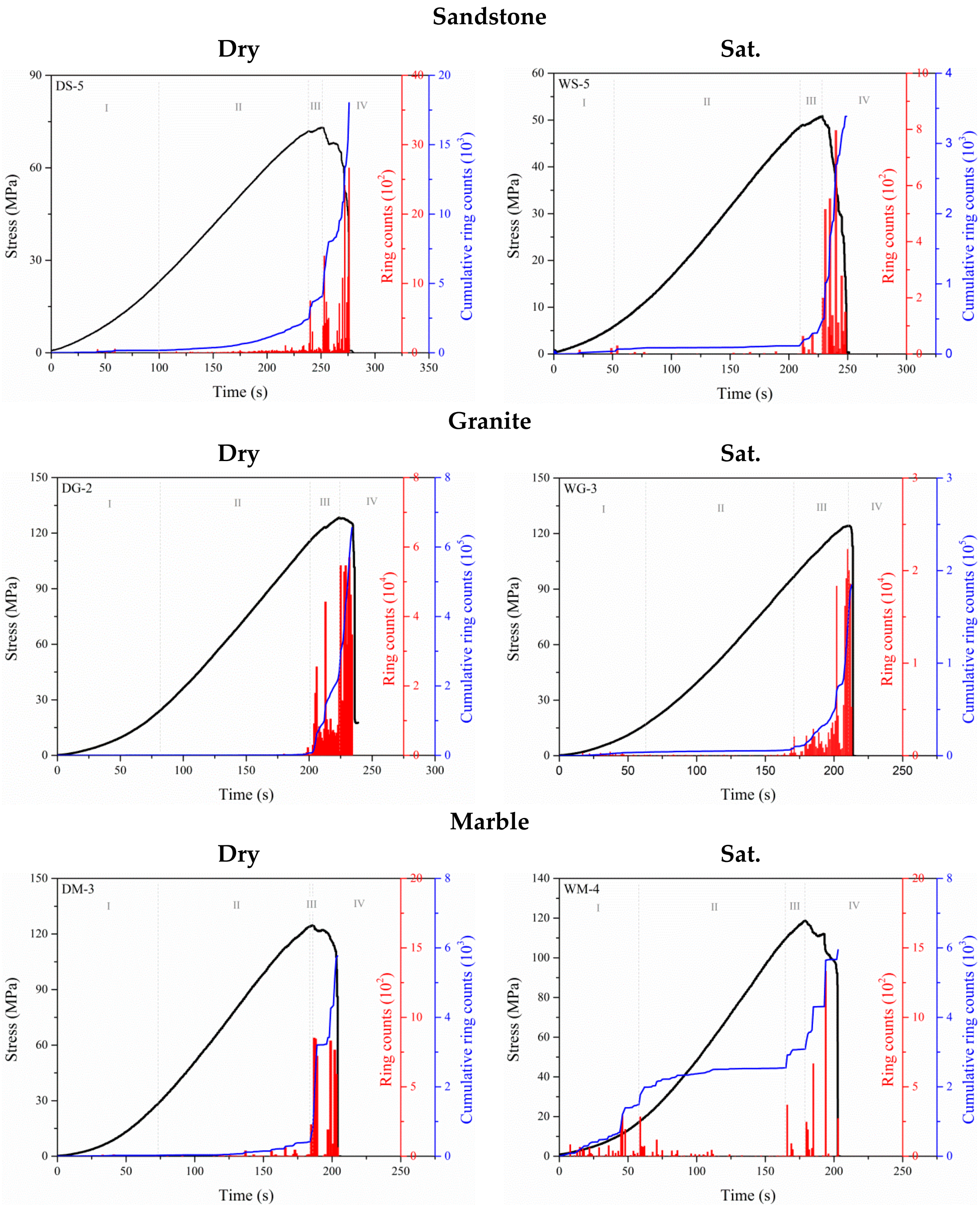

Figure 5. Variations of axial stress, ring counts and cumulative ring counts versus time for different rock types under dry and saturated conditions.

Figure 6 shows the relationship between stress and ring counts, from which the effect of water on the cumulative ring counts under uniaxial compression is observed:

(1) In crack closure stage, the ring counts of the dry sandstone were slightly less than that of the saturated one. On the contrary, for the granite and the marble, the number of ring counts in the saturated state was larger than that in dry state, indicating saturated specimens generate more microcracks during this stage.

(2) The stress at the onset of ring counts outburst, i.e., the transition point between stages II and III is defined as the threshold of crack damage [52]. For all rock types, the crack damage stress decreased when the rock became water-saturated. As an example, the crack damage stress of the dry granite specimen was approximately 115.72 MPa (90.1% of UCS), which was 1.20 times

greater than that of the saturated one (77.6% of UCS). This implies that the presence of water lowered the threshold of elastic energy release.

(3) The cumulative ring counts of dry rocks were dramatically greater than that of saturated ones, meaning that the rocks tested under dry conditions suffered more violent failures. This could be due to the increasing storage of elastic energy before failure, which can be reflected by the larger shaded area under the pre-peak portion of stress–strain curves. Another reason may be due to the higher slope of the stress drop in post-peak stage (i.e., greater unloading rate) causing a catastrophic fracture of the rock [53,54].

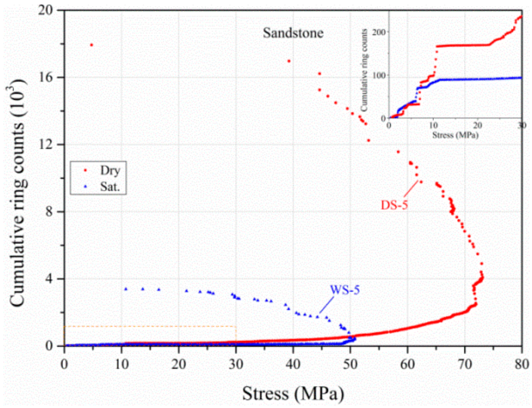

(**a**)

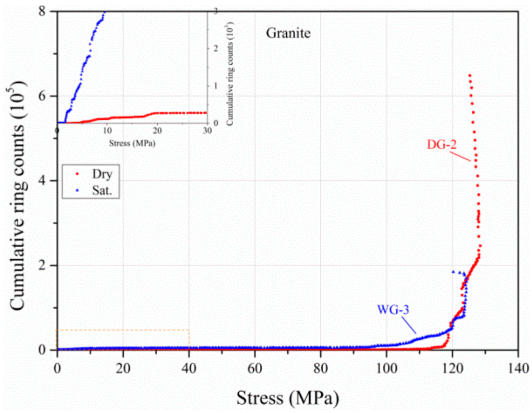

(**b**)

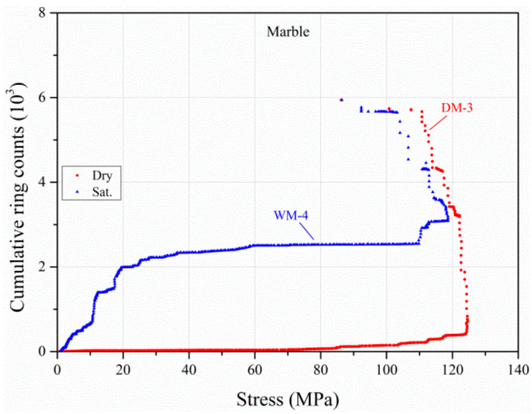

(**c**)

Figure 6. Variation of cumulative ring counts versus axial stress: (**a**) sandstone; (**b**) granite; and (**c**) marble.

3.2.2. Water Induced Variation in Microscale Crack Type

Ohtsu et al. [55] suggested a method to classify the crack type based on two AE parameters, namely the rise-time-to-amplitude (RA) ratio and the average frequency (AF, defined as counts/duration time). Generally, tensile cracks have higher AF and lower RA values while shear cracks possess lower AF and higher RA values. In this study, this method was adopted to identify the failure pattern. Figure 7 depicts the distribution of probability density of AF–RA data. The areas in red indicate higher density regions and the areas in blue represent lower density regions.

From Figure 7, we can clearly observe that for the dry sandstone, more AE signals are distributed above the diagonal and the maximum density region below the diagonal, meaning that it failed in a tensile-dominated mixed mode. However, for the saturated sandstone, the overwhelming majority of cracks concentrate under the diagonal, which suggests that its failure was characterized by shear fracture. This phenomenon indicates that the water presence transformed the sandstone failure type into shear mode, which agrees with previous studies on gabbro [20] and coal [19]. The change of the failure mode was possibly caused by the water-induced frictional reduction, which will be discussed latter.

Similarly, for the saturated granite, the areas in dark red move to the part below the diagonal, signifying that there were more shear microcracks after water saturation. However, under dry and saturated conditions, the majority of cracks for the marble were located in the tensile region. The presence of water seemed to not affect the failure mode of the marble.

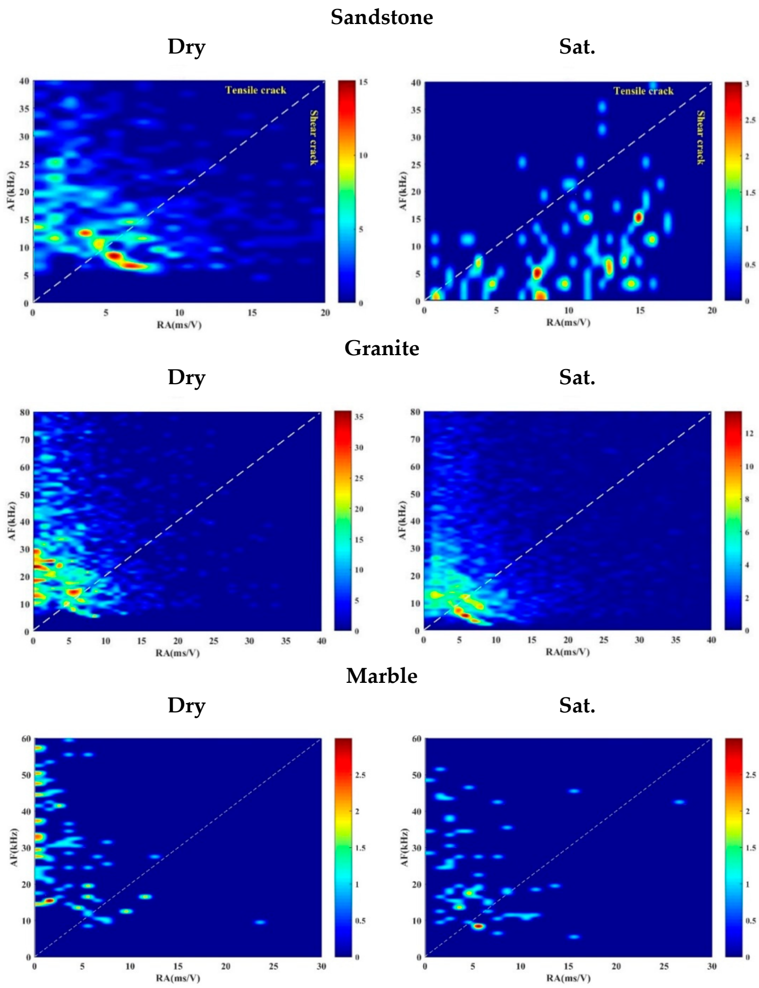

Figure 7. Probability density of rise time-to-amplitude ratio–average frequency (RA–AF) data for dry and saturated rocks.

4. Discussion

In this section, the weakening effects of water on the mechanical behavior of different rock types are interpreted from the following aspects.

4.1. Chemical and Physical Deterioration

When submerged in purified water, rocks will react with water chemically or physically in three manners.

(1) The hydrolysis of quartz. In the case of silicate rocks under conditions of moisture, water as a corrosive agent hydrolyzes the quartz minerals. The hydrolysis of Si–O–Si bond in quartz lowers the activation barrier to subcritical crack growth as strong Si–O–Si bonds at crack tips are replaced by weaker hydrogen bonds [35–38,48]:

$$(-Si - O - Si-) + (H - O - H) \rightleftharpoons (-Si - OH - HO - Si-). \tag{1}$$

At the same time, the increasing external stress inducing crack creation and propagation also promotes the quartz hydrolysis. Theoretically, the higher content of quartz leads to the greater UCS reduction due to water presence, as shown in Figure 8. Therefore, quartz hydrolysis plays an important role in weakening the UCS of the sandstone and the granite, while it is absent for the marble according to the mineral compositions of the three rock types listed in Table 1. From Figure 8, it is worth noting that the UCS reduction of granite is apparently lower than the predicted value, probably due to the hydrolysis of quartz being limited by its extremely low porosity (lower permeability).

(2) The swelling of clay minerals. It is well-known that expandable clay minerals (e.g., smectite) cause high swelling stresses after water absorption, further expanding existing microfractures as well as creating new micro-fractures [28,56]. The increase of crack density decreases the rock strength [57,58]. In this study, this effect only acts on the sandstone containing smectite.

(3) The dissolution of calcite. Calcite minerals are vulnerable to dissolution even in weak acidic environment [20,56,59,60], as:

$$CaCO_3 + CO_2 + H_2O \rightarrow 2HCO_3^- + Ca^{2+}. \tag{2}$$

This will increase the porosity of rock and decrease the intergranular cohesion, which results in the UCS reduction of the sandstone and the marble.

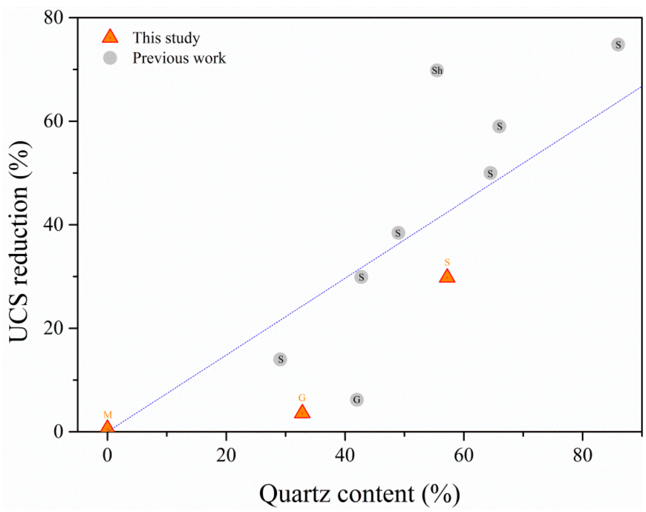

Figure 8. UCS reduction against quartz content (data from [4,6,25,61–64]). S, sandstone; G, granite; M, marble; Sh, shale.

4.2. The Increase of Pore Pressure

Pore-water pressure increases only when the test is performed under a drained condition [65], in which the water is unable to migrate freely within the testing time duration and hence the pore-water will be pressurized. The increase of pore pressure reduces the rock strength via two aspects: decreasing the effective normal compressive stress [47] and inducing microcrack damage once the pore pressure exceeds the tensile strength of rocks [40]. Whether the rock is tested in drained or un-drained condition can be identified by the fluid diffusion characteristic time (t_d), which is determined in a porous saturated material by the following equation [65,66]:

$$t_d = \frac{{d_m}^2}{H} \tag{3}$$

where d_m is the minimum distance from the specimen center to a free surface and H is the hydraulic diffusivity of this material. The hydraulic diffusivity is estimated by [67]:

$$H = \frac{\kappa B K}{\eta \alpha} \tag{4}$$

where κ is the permeability of the material; K is the bulk modulus of the porous material; η is the viscosity of fluid; B and α are the Skempton's and Biot's coefficients, respectively. In this study, d_m is 25 mm according to the specimen geometry. η for water is about 1×10^{-3} Pa·s. B and α are assumed to be of the order of unity [64,65]. κ and K are listed in Table 3. Therefore, the characteristic times for water diffusion of sandstone, granite and marble are 0.35, 222 and 2440 s, respectively, which are approximated to the predicted values, as shown in Figure 9. Apparently, t_d for the granite and the marble are higher than their failure times, in other words, the two rocks were tested under un-drained condition. The increasing pore pressure will induce severe crack damage [40,68] and lower the UCS of wet granite and marble specimens. In contrast, t_d for the sandstone is far below its average failure time (226 s), which suggests that pore pressure is limited due to the discharge of pore water. This can hereby interpret the phenomenon that the granite and the marble specimens in crack closure stage (Figure 6) generate more microcracks when they become water-saturated while the ring counts of saturated sandstone slightly decrease.

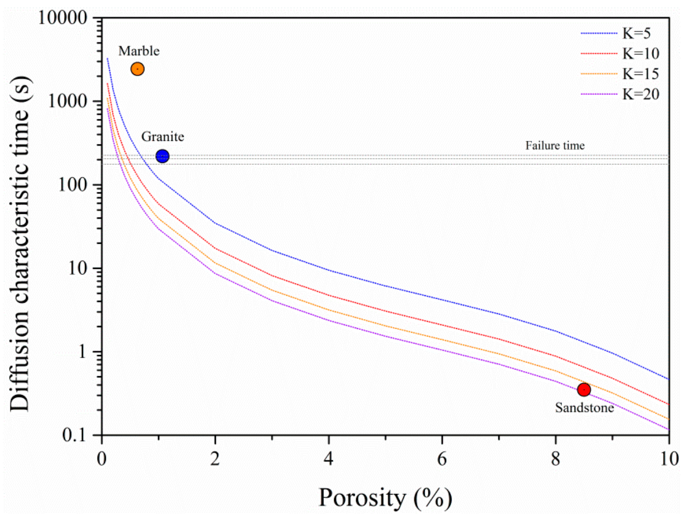

Figure 9. Predicted water diffusion characteristic time against porosity (the predicted lines are obtained according to Equations (3) and (4), in which the permeability of rock is approximated via rock porosity (ϕ): $\kappa = 31\phi + 7463\phi^2 + 191(10\phi)^{10}$); the fully filled symbols are the diffusion characteristic times for the three tested rocks).

4.3. Frictional Reduction

The frictional coefficient at grain boundaries will be reduced under saturated condition. This effect facilitates the initiation and slide of shear crack, further decreasing rock strength. Figure 10 shows the reduction in the friction coefficients of minerals due to water saturation. We can clearly observe that the percentage decreases are quite varied among different minerals. Generally, expandable minerals, such as smectite and kaolinite, exhibit great loss of friction coefficients in water-saturated condition. The reason may be that the surface of minerals attracts water molecules so as to form a thin water film with weak frictional strength [43–45]. However, for other minerals, the reductions in friction coefficients are relatively smaller. Particularly, the friction coefficients of quartz and feldspar even remain constant after water saturation. According to mineral contents and the loss percentages of friction coefficients, the effect of frictional reduction perhaps dominates the failure of saturated sandstone and granite but does not work in the marble. The failure types of the rocks, as explained in Section 3.2.2, lend support to this hypothesis.

Summarily, for the sandstone, the significant strength decrease is caused by the water-induced coupled effects of quartz hydrolysis, clay mineral swelling, calcite dissolution and frictional reduction. The quartz hydrolysis, pore pressure increase and friction reduction give rise to a moderate decrease in the strength of the granite. The least UCS reduction of the saturated marble may be attributed to the increase of pore pressure and the dissolution of calcite.

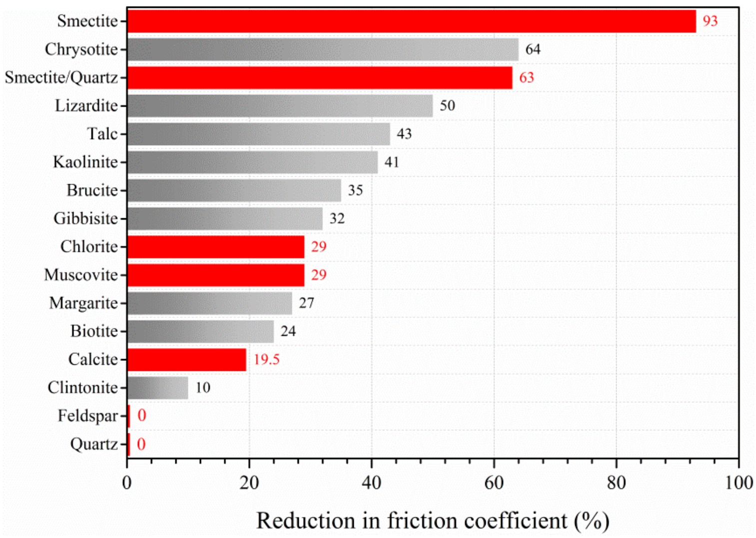

Figure 10. Water-induced reduction in friction coefficient for different minerals (data from [43–45,69]; the data indicate the corresponding minerals comprising the tested rocks).

5. Conclusions

In order to investigate the water-weakening effects on mechanical behavior and reveal the weakening mechanisms for different rock types, a series of uniaxial compression tests was carried out on three kinds of rocks (i.e., sandstone, granite and marble) in oven-dried and water-saturated states. Mechanical parameters, such as UCS, elastic modulus and critical strain, were obtained and compared. AE technique was also used to monitor and record the evolution of ring counts during loading process. The failure pattern was identified by the correlation between RA and AF values.

The UCS, elastic modulus and critical strain of rocks decrease after water saturation. The weakening degree varies with rock type: the mechanical properties of the sandstone are the most susceptible to water, followed by the granite and the marble.

In crack closure stage, the saturated sandstone specimen cumulates less ringing counts than the dry one, while more ringing counts are generated in the saturated state for the granite and the marble. This depends on which condition the specimen is tested in (drained or un-drained). The pore-water lowers the crack damage threshold of rocks. Additionally, in post-peak stage, the ringing counts of dry specimens are much greater than those of saturated specimens.

According to the RA–AF relationship, the failure of the three rocks is dominated by tensile cracks in a dry state. When tested under saturated conditions, more shear cracks occur in the sandstone and the granite, probably due to the water-induced frictional reduction. However, water has no effect on the failure pattern of the marble.

The coupled effects of quartz hydrolysis, clay mineral swelling, calcite dissolution and frictional reduction are responsible for the notable strength drop of the sandstone. The mild strength decrease of granite is mainly caused by the quartz hydrolysis, pore pressure increase and friction reduction. The pore pressure and calcite dissolution only cause slight reduction in the UCS of the saturated marble.

Author Contributions: X.C. and Z.Z. conceived and designed the tests; X.C. and H.Z. proposed and participated in the mechanical experiments and processed the data; X.D. conducted the XRD tests; X.C. wrote the paper; X.C. and K.L. revised the paper.

Funding: This research was funded by the National Basic Research Program of China, grant number 2015CB060200, the National Natural Science Foundation of China, grant number 41772313, the Natural Science Foundation of Hunan, grant number 2015JJ4067 and the Graduated Students' Research and Innovation Fund Project of Central South University grant number 2018zzts210.

Acknowledgments: The authors wish to thank Yizhong Luo from the Advanced Research Center in Central South University, and Yin Chang from the School of Resources and Safety Engineering in Central South University for their help in experiments.

Conflicts of Interest: The authors declare no conflict of interest.

References

1. Hawkins, A.B.; McConnell, B.J. Sensitivity of sandstone strength and deformability to changes in moisture content. *Q. J. Eng. Geol. Hydrogeol.* **1992**, *25*, 115–130. [CrossRef]
2. Erguler, Z.A.; Ulusay, R. Water-induced variations in mechanical properties of clay-bearing rocks. *Int. J. Rock Mech. Min. Sci.* **2009**, *46*, 355–370. [CrossRef]
3. Yilmaz, I. Influence of water content on the strength and deformability of gypsum. *Int. J. Rock Mech. Min. Sci.* **2010**, *47*, 342–347. [CrossRef]
4. Zhou, Z.; Cai, X.; Cao, W.; Li, X.; Xiong, C. Influence of Water Content on Mechanical Properties of Rock in Both Saturation and Drying Processes. *Rock Mech. Rock Eng.* **2016**, *49*, 3009–3025. [CrossRef]
5. Wasantha, P.L.P.; Ranjith, P.G. Water-weakening behavior of Hawkesbury sandstone in brittle regime. *Eng. Geol.* **2014**, *178*, 91–101. [CrossRef]
6. Zhou, Z.; Cai, X.; Ma, D.; Du, X.; Chen, L.; Wang, H.; Zang, H. Water saturation effects on dynamic fracture behavior of sandstone. *Int. J. Rock Mech. Min. Sci.* **2019**, *114*, 46–61. [CrossRef]
7. Wong, L.N.Y.; Maruvanchery, V.; Liu, G. Water effects on rock strength and stiffness degradation. *Acta Geotech.* **2016**, *11*, 713–737. [CrossRef]
8. Iverson, R.M. Landslide triggering by rain infiltration. *Water Resour. Res.* **2000**, *36*, 1897–1910. [CrossRef]
9. Ma, D.; Cai, X.; Li, Q.; Duan, H. In-Situ and Numerical Investigation of Groundwater Inrush Hazard from Grouted Karst Collapse Pillar in Longwall Mining. *Water* **2018**, *10*, 1187. [CrossRef]
10. Lu, C.; Zilong, Z.; Chuanwei, Z.; Ling, Z.; Yuan, Z. Failure pattern of large-scale goaf collapse and a controlled roof caving method used in gypsum mine. *Geomech. Eng.* **2019**, *18*, 449–457.
11. Zang, A.; Zimmermann, G.; Hofmann, H.; Stephansson, O.; Min, K.-B.; Kim, K.Y. How to Reduce Fluid-Injection-Induced Seismicity. *Rock Mech. Rock Eng.* **2015**, *34*, 249–260. [CrossRef]
12. Ma, D.; Duan, H.; Liu, J.; Li, X.; Zhou, Z. The role of gangue on the mitigation of mining-induced hazards and environmental pollution: An experimental investigation. *Sci. Total Environ.* **2019**, *664*, 436–448. [CrossRef] [PubMed]
13. Ma, D.; Duan, H.; Li, X.; Li, Z.; Zhou, Z.; Li, T. Effects of seepage-induced erosion on nonlinear hydraulic properties of broken red sandstones. *Tunn. Undergr. Space Technol.* **2019**, *91*, 102993. [CrossRef]
14. Török, Á.; Vásárhelyi, B. The influence of fabric and water content on selected rock mechanical parameters of travertine, examples from Hungary. *Eng. Geol.* **2010**, *115*, 237–245. [CrossRef]

15. Dyke, C.G.; Dobereiner, L. Evaluating the strength and deformability of sandstones. *Q. J. Eng. Geol. Hydrogeol.* **1991**, *24*, 123–134. [CrossRef]
16. Jiang, Q.; Cui, J.; Feng, X.; Jiang, Y. Application of computerized tomographic scanning to the study of water-induced weakening of mudstone. *Bull. Eng. Geol. Environ.* **2014**, *73*, 1293–1301. [CrossRef]
17. Zang, A.; Wagner, C.F.; Dresen, G. Acoustic emission, microstructure, and damage model of dry and wet sandstone stressed to failure. *J. Geophys. Res. Solid Earth* **1996**, *101*, 17507–17521. [CrossRef]
18. Li, H.; Shen, R.; Li, D.; Jia, H.; Li, T.; Chen, T.; Hou, Z. Acoustic Emission Multi-Parameter Analysis of Dry and Saturated Sandstone with Cracks under Uniaxial Compression. *Energies* **2019**, *12*, 1959. [CrossRef]
19. Yao, Q.; Chena, T.; Tang, C.; Sedighic, M.; Wang, S.; Huang, Q. Influence of moisture on crack propagation in coal and its failure modes. *Eng. Geol.* **2019**, *258*, 2019. [CrossRef]
20. Liu, X.; Wu, L.; Zhang, Y.; Liang, Z.; Yao, X.; Liang, P. Frequency properties of acoustic emissions from the dry and saturated rock. *Environ. Earth Sci.* **2019**, *78*, 67. [CrossRef]
21. Yao, Q.; Li, X.; Zhou, J.; Ju, M.; Chong, Z.; Zhao, B. Experimental study of strength characteristics of coal specimens after water intrusion. *Arab. J. Geosci.* **2015**, *8*, 6779–6789. [CrossRef]
22. Yao, Q.; Chen, T.; Ju, M.; Liang, S.; Liu, Y.; Li, X. Effects of Water Intrusion on Mechanical Properties of and Crack Propagation in Coal. *Rock Mech. Rock Eng.* **2016**, *49*, 4699–4709. [CrossRef]
23. Ranjith, P.G.; Jasinge, D.; Song, J.Y.; Choi, S.K. A study of the effect of displacement rate and moisture content on the mechanical properties of concrete: Use of acoustic emission. *Mech. Mater.* **2008**, *40*, 453–469. [CrossRef]
24. Hashiba, K.; Fukui, K.; Kataoka, M.; Chu, S.Y. Effect of water on the strength and creep lifetime of andesite. *Int. J. Rock Mech. Min. Sci.* **2018**, *108*, 37–42. [CrossRef]
25. Miao, S.; Cai, M.; Guo, Q.; Wang, P.; Liang, M. Damage effects and mechanisms in granite treated with acidic chemical solutions. *Int. J. Rock Mech. Min. Sci.* **2016**, *88*, 77–86. [CrossRef]
26. Aydan, Ö.; Ulusay, R. Geomechanical evaluation of derinkuyu antique underground city and its implications in geoengineering. *Rock Mech. Rock Eng.* **2013**, *46*, 731–754. [CrossRef]
27. Hadizadeh, J.; Law, R.D. Water-weakening of sandstone and quartzite deformed at various stress and strain rates. *Int. J. Rock Mech. Min. Sci.* **1991**, *28*, 431–439. [CrossRef]
28. Wasantha, P.L.P.; Ranjith, P.G.; Permata, G.; Bing, D. Damage evolution and deformation behaviour of dry and saturated sandstones: Insights gleaned from optical measurements. *Meas. J. Int. Meas. Confed.* **2018**, *130*, 8–17. [CrossRef]
29. Rajabzadeh, M.A.; Moosavinasab, Z.; Rakhshandehroo, G. Effects of rock classes and porosity on the relation between uniaxial compressive strength and some rock properties for carbonate rocks. *Rock Mech. Rock Eng.* **2012**, *45*, 113–122. [CrossRef]
30. Gholami, R.; Rasouli, V. Mechanical and elastic properties of transversely isotropic slate. *Rock Mech. Rock Eng.* **2014**, *47*, 1763–1773. [CrossRef]
31. Zhang, Q.B.; Zhao, J. A review of dynamic experimental techniques and mechanical behaviour of rock materials. *Rock Mech. Rock Eng.* **2014**, *47*, 1411–1478. [CrossRef]
32. Zhou, Z.; Cai, X.; Zhao, Y.; Chen, L.; Xiong, C.; Li, X. Strength characteristics of dry and saturated rock at different strain rates. *Trans. Nonferrous Met. Soc. China* **2016**, *26*, 1919–1925. [CrossRef]
33. Hammond, M.L.; Ravitz, S.F. Influence of Environment on Brittle Fracture of Silica. *J. Am. Ceram. Soc.* **1963**, *46*, 329–332. [CrossRef]
34. Vutukuri, V.S. The effect of liquids on the tensile strength of limestone. *Int. J. Rock Mech. Min. Sci.* **1974**, *11*, 27–29. [CrossRef]
35. Michalske, T.A.; Freiman, S.W. A molecular interpretation of stress corrosion in silica. *Nature* **1982**, *295*, 511–512. [CrossRef]
36. Freiman, S.W. Effects of chemical environments on slow crack growth in glasses and ceramics. *J. Geophys. Res. Solid Earth* **1984**, *89*, 4072–4076. [CrossRef]
37. Eppes, M.C.; Keanini, R. Mechanical weathering and rock erosion by climate-dependent subcritical cracking. *Rev. Geophys.* **2017**, *55*, 470–508. [CrossRef]
38. Atkinson, B.K.; Meredith, P.G. Stress corrosion cracking of quartz: A note on the influence of chemical environment. *Tectonophysics* **1981**, *77*, T1–T11. [CrossRef]
39. Handin, J.; Rex, V.; Hager, J.; Melvin, F.; Feather, J.N. Experimental Deformation of Sedimentary Rocks Under Confining Pressure: Pore Pressure Tests. *Am. Assoc. Pet. Geol. Bull.* **1963**, *47*, 717–755.

40. Zhong, C.; Zhang, Z.; Ranjith, P.G.; Lu, Y.; Choi, X. The role of pore water plays in coal under uniaxial cyclic loading. *Eng. Geol.* **2019**, *257*, 105125. [CrossRef]
41. Homand, S.; Shao, J.F. Mechanical behaviour of a porous chalk and effect of saturating fluid. *Mech. Cohesive-Frictional Mater.* **2000**, *5*, 583–606. [CrossRef]
42. Van Eeckhout, E.M. The mechanisms of strength reduction due to moisture in coal mine shales. *Int. J. Rock Mech. Min. Sci. Geomech.* **1976**, *13*, 61–67. [CrossRef]
43. Morrow, C.A.; Moore, D.E.; Lockner, D.A. The effect of mineral bond strength and adsorbed water on fault gouge frictional strength. *Geophys. Res. Lett.* **2000**, *27*, 815–818. [CrossRef]
44. Moore, D.E. Crystallographic controls on the frictional behavior of dry and water-saturated sheet structure minerals. *J. Geophys. Res.* **2004**, *109*, B03401. [CrossRef]
45. Kawai, K.; Sakuma, H.; Katayama, I.; Tamura, K. Frictional characteristics of single and polycrystalline muscovite and influence of fluid chemistry. *J. Geophys. Res. Solid Earth* **2015**, *120*, 6209–6218. [CrossRef]
46. Kang, J.Q.; Zhu, J.B.; Zhao, J. A review of mechanisms of induced earthquakes: From a view of rock mechanics. *Geomech. Geophys. Geo-Energy Geo-Resour.* **2019**, *5*, 171–196. [CrossRef]
47. Mcconnell, B.J. Factors Controlling Sandstone Strength and Deformability in Uniaxial Compression. Ph.D. Thesis, University of Bristol, Bristol, UK, 1989.
48. Zhou, Z.; Cai, X.; Ma, D.; Cao, W.; Chen, L.; Zhou, J. Effects of water content on fracture and mechanical behavior of sandstone with a low clay mineral content. *Eng. Fract. Mech.* **2018**, *193*, 47–65. [CrossRef]
49. Wang, S.; Li, X.; Yao, J.; Gong, F.; Li, X.; Du, K.; Tao, M.; Huang, L.; Du, S. Experimental investigation of rock breakage by a conical pick and its application to non-explosive mechanized mining in deep hard rock. *Int. J. Rock Mech. Min. Sci.* **2019**, *122*, 104063. [CrossRef]
50. Song, Z.; Konietzky, H.; Herbst, M. Bonded-particle model-based simulation of artificial rock subjected to cyclic loading. *Acta Geotech.* **2019**, *14*, 955–971. [CrossRef]
51. Ma, D.; Wang, J.; Cai, X.; Ma, X.; Zhang, J.; Zhou, Z.; Tao, M. Effects of height/diameter ratio on failure and damage properties of granite under coupled bending and splitting deformation. *Eng. Fract. Mech.* **2019**, *220*, 106640. [CrossRef]
52. Martin, C.D.; Chandler, N.A. The progressive fracture of Lac du Bonnet granite. *Int. J. Rock Mech. Min. Sci.* **1994**, *31*, 643–659. [CrossRef]
53. Zhao, X.G.; Wang, J.; Cai, M.; Cheng, C.; Ma, L.K.; Su, R.; Zhao, F.; Li, D.J. Influence of unloading rate on the strainburst characteristics of beishan granite under true-triaxial unloading conditions. *Rock Mech. Rock Eng.* **2014**, *47*, 467–483. [CrossRef]
54. Tao, M.; Li, X.; Wu, C. Characteristics of the unloading process of rocks under high initial stress. *Comput. Geotech.* **2012**, *45*, 83–92. [CrossRef]
55. Ohtsu, M.; Isoda, T.; Tomoda, Y. Acoustic Emission Techniques Standardized for Concrete Structures. *J. Acoust. Emiss.* **2007**, *25*, 21–32.
56. Ahamed, M.A.A.; Perera, M.S.A.; Matthai, S.K.; Ranjith, P.G.; Dong-yin, L. Journal of Petroleum Science and Engineering Coal composition and structural variation with rank and its influence on the coal-moisture interactions under coal seam temperature conditions—A review article. *J. Pet. Sci. Eng.* **2019**, *180*, 901–917. [CrossRef]
57. Zhou, Z.; Cai, X.; Ma, D.; Chen, L.; Wang, S.; Tan, L. Dynamic tensile properties of sandstone subjected to wetting and drying cycles. *Constr. Build. Mater.* **2018**, *182*, 215–232. [CrossRef]
58. Zhou, Z.; Cai, X.; Li, X.; Cao, W.; Du, X. Dynamic Response and Energy Evolution of Sandstone Under Coupled Static—ynamic Compression: Insights from Experimental Study into Deep Rock Engineering Applications. *Rock Mech. Rock Eng.* **2019**, 1–27. [CrossRef]
59. Ciantia, M.O.; Castellanza, R.; di Prisco, C. Experimental Study on the Water-Induced Weakening of Calcarenites. *Rock Mech. Rock Eng.* **2014**, *48*, 441–461. [CrossRef]
60. Ciantia, M.O.; Castellanza, R.; Crosta, G.B.; Hueckel, T. Efects of mineral suspension and dissolution on strength and compressibility of soft carbonate rocks. *Eng. Geol.* **2015**, *184*, 1–18. [CrossRef]
61. Qiao, L.; Wang, Z.; Huang, A. Alteration of Mesoscopic Properties and Mechanical Behavior of Sandstone Due to Hydro-Physical and Hydro-Chemical Effects. *Rock Mech. Rock Eng.* **2017**, *50*, 255–267. [CrossRef]
62. Lyu, Q.; Long, X.; Ranjith, P.G.; Tan, J.; Kang, Y. Experimental investigation on the mechanical behaviours of a low-clay shale under water-based fluids. *Eng. Geol.* **2018**, *233*, 124–138. [CrossRef]

63. Verstrynge, E.; Adriaens, R.; Elsen, J.; Van Balen, K. Multi-scale analysis on the influence of moisture on the mechanical behavior of ferruginous sandstone. *Constr. Build. Mater.* **2014**, *54*, 78–90. [CrossRef]
64. Masoumi, H.; Horne, J.; Timms, W. Establishing Empirical Relationships for the Effects of Water Content on the Mechanical Behavior of Gosford Sandstone. *Rock Mech. Rock Eng.* **2017**, *50*, 2235–2242. [CrossRef]
65. Nicolas, A.; Fortin, J.; Regnet, J.B.; Dimanov, A.; Gúeguen, Y. Brittle and semi-brittle behaviours of a carbonate rock: Influence of water and temperature. *Geophys. J. Int.* **2016**, *206*, 438–456. [CrossRef]
66. Duda, M.; Renner, J. The weakening effect of water on the brittle failure strength of sandstone. *Geophys. J. Int.* **2013**, *192*, 1091–1108. [CrossRef]
67. Kümpel, H. Poroelasticity: Parameters reviewed. *Geophys. J. Int.* **1991**, *105*, 783–799. [CrossRef]
68. Aben, F.M.; Doan, M.L.; Gratier, J.P.; Renard, F. High strain rate deformation of porous sandstone and the asymmetry of earthquake damage in shallow fault zones. *Earth Planet. Sci. Lett.* **2017**, *463*, 81–91. [CrossRef]
69. Ikari, M.J.; Saffer, D.M.; Marone, C. Effect of hydration state on the frictional properties of montmorillonite-based fault gouge. *J. Geophys. Res. Solid Earth* **2007**, *112*, B06423. [CrossRef]